

**Microstructure and magnetostriction of Tb 0.3 Dy 0.7 Fe 1.95 prepared under different solidification conditions by zoning and modified Bridgman techniques**

Mithun Palit, S. Pandian, R. Balamuralikrishnan, A. K. Singh, Niranjana Das, V. Chandrasekharan, and G. Markandeyulu

Citation: *Journal of Applied Physics* **100**, 074913 (2006); doi: 10.1063/1.2356913

View online: <http://dx.doi.org/10.1063/1.2356913>

View Table of Contents: <http://scitation.aip.org/content/aip/journal/jap/100/7?ver=pdfcov>

Published by the [AIP Publishing](#)

---

**Articles you may be interested in**

[Dual-resonance converse magnetoelectric and voltage step-up effects in laminated composite of long-type 0.71Pb\(Mg<sub>1/3</sub>Nb<sub>2/3</sub>\)O<sub>3</sub>-0.29PbTiO<sub>3</sub> piezoelectric single-crystal transformer and Tb<sub>0.3</sub>Dy<sub>0.7</sub>Fe<sub>1.92</sub> magnetostrictive alloy bars](#)

*J. Appl. Phys.* **109**, 104103 (2011); 10.1063/1.3587574

[Effect of B on the microstructure and magnetostriction of zoned Dy 0.7 Tb 0.3 Fe 1.95](#)

*J. Appl. Phys.* **101**, 09C512 (2007); 10.1063/1.2711610

[Magnetoelasticity of Tb 0.3 Dy 0.7 Fe 1.95 alloys in a multiaxial stress-magnetic field space](#)

*Appl. Phys. Lett.* **90**, 182505 (2007); 10.1063/1.2736300

[Magnetostriction and electrical resistivity of Si doped Tb 0.3 Dy 0.7 Fe 1.95 oriented crystals](#)

*Appl. Phys. Lett.* **89**, 192507 (2006); 10.1063/1.2384800

[Microstructure and magnetostrictive properties of Tb-Dy-Fe \(Al\) alloys](#)

*J. Appl. Phys.* **87**, 6295 (2000); 10.1063/1.372684

---



# Microstructure and magnetostriction of $Tb_{0.3}Dy_{0.7}Fe_{1.95}$ prepared under different solidification conditions by zoning and modified Bridgman techniques

Mithun Palit, S. Pandian,<sup>a)</sup> R. Balamuralikrishnan, A. K. Singh, Niranjan Das, and V. Chandrasekharan

*Defence Metallurgical Research Laboratory, Hyderabad 500 058, India*

G. Markandeyulu

*Indian Institute of Technology Madras, Chennai 600 036, India*

(Received 3 April 2006; accepted 14 July 2006; published online 12 October 2006)

An intermetallic compound of nominal composition  $Tb_{0.3}Dy_{0.7}Fe_{1.95}$  was conventionally cast in the form of cylindrical rods of 8 mm diameter and directionally solidified by zoning at three different growth rates. Compounds of the same nominal composition were also directionally solidified in the form of cylindrical rods of 20 mm diameter by modified Bridgman technique, at two different growth rates. The microstructure of the directionally solidified compounds has been investigated as a function of solidification rate and compared with that of conventionally cast compound. The observed microstructural features of these samples have been correlated with the magnetostriction measured on the corresponding samples. Further, by examining the longitudinal sections cut along its cylindrical axis, a correlation of microstructure with magnetostriction has been brought out for each directionally solidified sample as a function of distance from the initially solidified end to the other. It has been observed that a large magnetostriction (at 4.5 kOe) and a high initial slope of magnetostriction versus applied magnetic field are realized in the directionally solidified samples as compared to the conventionally cast sample. An improvement in the property has been observed among the directionally solidified samples when solidified with higher growth rates. It is surmised on the basis of the observed microstructural features in this study that a large magnetostriction is realized if formation of  $(Tb, Dy)Fe_2$  occurs by congruent solidification rather than by the peritectic reaction  $L + (Tb, Dy)Fe_3 \rightarrow (Tb, Dy)Fe_2$ . © 2006 American Institute of Physics.

[DOI: [10.1063/1.2356913](https://doi.org/10.1063/1.2356913)]

## I. INTRODUCTION

The anisotropy compensated  $(Tb_xDy_{1-x})Fe_{2-y}$  intermetallic compounds with  $x \sim 0.3$  and  $y \sim 0.03-0.1$  exhibit a large room temperature magnetostriction<sup>1,2</sup> and are generally grown in the form of cylindrical rods by adopting directional solidification (DS) methods of either zoning<sup>3</sup> (up to a diameter of  $\sim 8$  mm) or modified Bridgman<sup>4</sup> (for larger diameter, typically  $> 15$  mm) technique. Efforts have been on<sup>5-11</sup> for achieving a large magnetostriction ( $\lambda$ ) and high magnetomechanical coupling coefficient ( $k_{33}$ ) over a wide temperature range. One of the means is through substitutions aimed at (i) extending the near zero magnetocrystalline anisotropy to a wide temperature range,<sup>7</sup> and (ii) evolving a microstructure consisting of mainly the magnetostrictive Laves phase,  $(Tb, Dy)Fe_2$  with  $(Tb, Dy)$  rich as a minor phase distributed in the intergranular regions. On the other hand, in the material processing, the main emphasis is placed on achieving sharp and uniform texture throughout the sample in order to realize a large and uniform (along the length) magnetostrictive strain at low applied magnetic fields. Therefore, the uniformity of texture is critical and a greater interest in

interrelating the measured magnetomechanical properties with grain orientation and microstructural features.<sup>8-11</sup> Some of the key parameters that have a profound effect on the texture and the microstructure in this material system are composition, method of premelting and casting, and directional solidification conditions such as solidification rate, temperature, gradient, etc. Earlier investigators<sup>10-12</sup> have used arc melted precast cylindrical samples for zoning, whereas in the current work, the precast rod samples have been prepared by vacuum induction melting and casting. While the temperature gradient is assumed to be constant in zoning (Z) technique, a gradual variation in the gradient is expected to prevail in the modified Bridgman (MB) technique. Thus an investigation involving both zoning and MB allows one to comparatively assess the effect of the temperature gradient on the resultant microstructure and subsequently correlate these to the magnetomechanical properties. In each of these techniques, samples have been grown at different solidification rates and characterized for the magnetostrictive properties. Further, to assess the extent of property uniformity in the DS samples, longitudinal sections of the samples as a function of distance from one end (initial solidification) have been studied. The results of these investigations are presented and discussed in this paper.

<sup>a)</sup>Author to whom correspondence should be addressed; FAX: +91-40-24340884; electronic mail: [pands@sify.com](mailto:pands@sify.com)

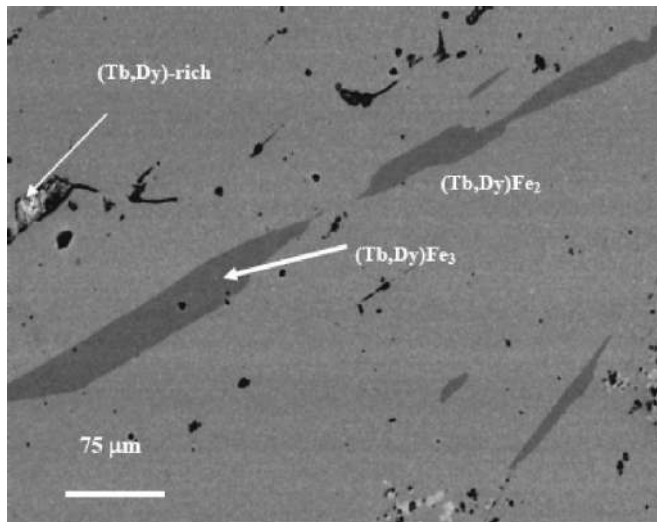


FIG. 1. Back scattered electron (BSE) image of the transverse section of the conventionally cast  $Tb_{0.3}Dy_{0.7}Fe_{1.95}$ .

## II. EXPERIMENTAL DETAILS

As mentioned earlier, directional solidification experiments in this study were carried out by zoning and modified Bridgman techniques. The compound  $Tb_{0.3}Dy_{0.7}Fe_{1.95}$  was prepared by melting the elements (Tb, Dy >99.5% purity; Fe >99.9% purity) in a recrystallized alumina crucible using a vacuum induction melting furnace and casting the molten compound in quartz tubes of 8 mm diameter. The conventionally cast (CC) rods were then sealed in quartz tubes under vacuum and zoned at three different speeds, namely, 18 cm/h (Z1), 36 cm/h (Z2), and 72 cm/h (Z3), using an induction coil powered at 450 kHz.

The directional solidification of the  $Tb_{0.3}Dy_{0.7}Fe_{1.95}$  compound by MB technique was performed by first preparing the compound in a vacuum induction melting furnace and then pouring the melt into a preheated (1350 °C) open ended 20 mm diameter quartz tube provided with a water-cooled chill plate at the bottom. The compound was then directionally solidified by lowering the mould from the hot zone at controlled withdrawal rates of 14 cm/h (MB1) and 70 cm/h (MB2).

The microstructural investigations on the sample surface parallel and perpendicular to the direction of solidification, i.e., on longitudinal and transverse sections, respectively, were carried out using optical and scanning electron microscope [Leo 440i scanning electron microscope (SEM) with Oxford energy dispersive spectroscopy (EDS) detector with a resolution of 136 eV at Mn  $K\alpha$ ]. The sample surfaces were prepared using standard metallographic technique and etched with Vilella's reagent (95 ml methanol+5 ml HCl+1 g picric acid) for optical microscopy. The x-ray diffraction (XRD) of the samples was performed using a Philips (model 3020) x-ray diffraction unit and the magnetostriction parallel to the growth direction was measured under dc magnetic field using temperature and field compensated resistance strain gauges.

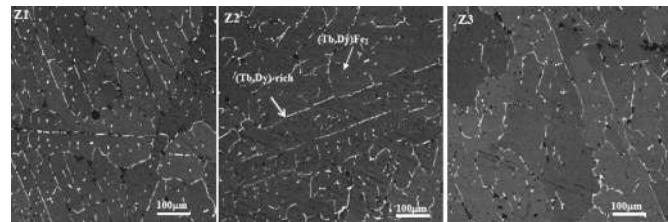


FIG. 2. BSE image of the transverse section of the samples Z1, Z2, and Z3 zoned at 18, 36, and 72 cm/h, respectively, showing the presence of  $(Tb,Dy)Fe_2$  and  $(Tb,Dy)$ -rich phases.

## III. RESULTS AND DISCUSSIONS

### A. Microstructure

The compound selected for the investigation is slightly rare earth rich relative to the stoichiometric  $(Tb,Dy)Fe_2$  phase. Assuming that the Tb–Dy–Fe system behaves as pseudobinary  $(Tb,Dy)$ –Fe, the composition at room temperature corresponds to a two phase [ $(Tb,Dy)Fe_2$  and  $(Tb,Dy)$  rich] region of the binary phase diagram.<sup>13,14</sup> However, the microstructure (Fig. 1) of the conventionally cast  $Tb_{0.3}Dy_{0.7}Fe_{1.95}$  shows the presence of peritectic  $(Tb,Dy)Fe_3$  phase in addition to the expected  $(Tb,Dy)Fe_2$  and  $(Tb,Dy)$ -rich phases. In contrast, the zoned samples exhibit (Fig. 2) the presence of these two phases only. The microstructure (Fig. 3) of the longitudinal sections of the samples zoned at different rates exhibits cellular  $(Tb,Dy)Fe_2$  grain morphology at lower zoning speed, and progressively changes to dendritic as the zoning speed is increased. For the samples directionally solidified by modified Bridgman technique, the volume fraction of the peritectic  $(Tb,Dy)Fe_3$  phase formed appears to depend on the rate of solidification and the temperature gradient. At a lower solidification rate (14 cm/h),  $(Tb,Dy)Fe_3$  is observed (Fig. 4) throughout the length of the sample (MB1), whereas at the higher rate (70 cm/h), the formation of  $(Tb,Dy)Fe_3$  seems to be suppressed up to about 40 mm away from the chilled end. Further away from 40 mm,  $(Tb,Dy)Fe_3$  phase starts appearing with a progressively increasing volume fraction as the distance from the chilled end increases.

The solidification sequences as inferred from the present study of different samples are described in Table I and compared with the solidification sequence under equilibrium condition. Depending on the absence/presence of  $(Tb,Dy)Fe_3$  phase, it is observed that the  $(Tb,Dy)Fe_2$  phase forms either congruently from the liquid or through a peritectic reaction depending on the prevalent solidification conditions. The presence of  $(Tb,Dy)Fe_3$  in the microstructure occurring at

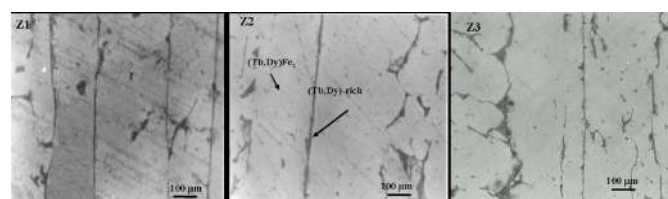


FIG. 3. Optical micrograph of longitudinal section of zoned samples, showing the transition of cellular to dendritic morphology of  $(Tb,Dy)Fe_2$  phase with increase in solidification rate.

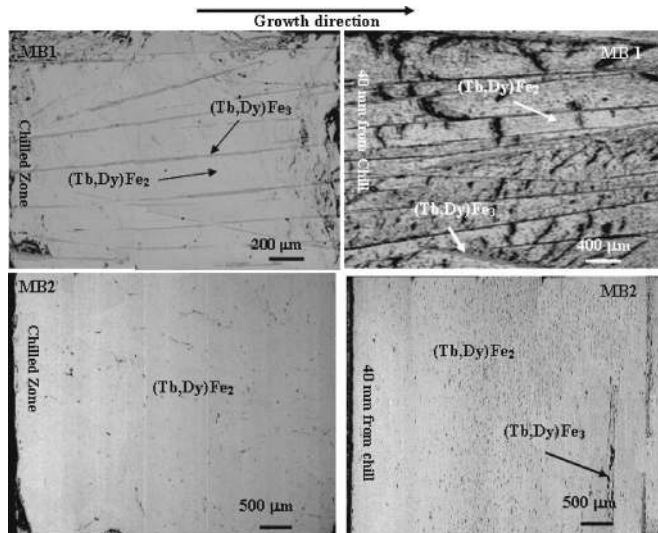


FIG. 4. Longitudinal sections of samples grown at 14 cm/h(MB1) and 70 cm/h(MB2) by modified Bridgman technique depicting the formation of (Tb,Dy)Fe<sub>3</sub> at lower solidification rate.

intergranular/cellular boundaries of the main (Tb,Dy)Fe<sub>2</sub> phase suggests an incomplete reaction (as is common in most reactions of peritectic type). The phase selection theory proposed by Umeda *et al.*<sup>15</sup> on peritectic solidification can be considered to discuss the solidification sequence as given in Table I. The theory explains the stability of growth of the competing phases on the basis of their corresponding solid-liquid interface temperatures, which is a function of temperature gradient and growth rate prevalent during solidification. According to the theory, the phase possessing higher interface temperature attains stability of growth over the other competing phases. It is proposed that if the rate of solidification exceeds a critical velocity ( $V_{tr}$ ) for a given thermal gradient, then the interface temperature of the peritectic (Tb,Dy)Fe<sub>2</sub> phase exceeds that of (Tb,Dy)Fe<sub>3</sub> phase. Under such conditions, (Tb,Dy)Fe<sub>2</sub> can form congruently from the liquid. As the thermal gradient increases,  $V_{tr}$  decreases, facilitating the formation of (Tb,Dy)Fe<sub>2</sub> directly from the liquid even at lower solidification rates. In zoning, high thermal gradient always prevails owing to good thermal conductivity of the sample and rapid conduction of heat from the thin layer of the liquid puddle. Therefore, it is supposed that the critical velocity ( $V_{tr}$ ) for the congruent formation of

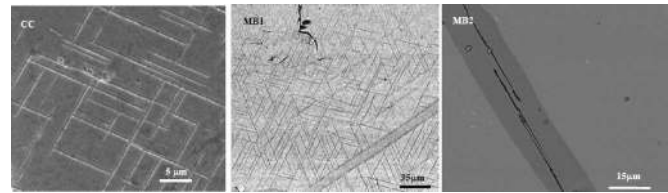


FIG. 5. Secondary electron (SE) image of CC and BSE image of MB1 revealing the formation of WSP of (Tb,Dy)Fe<sub>3</sub> phase. The BSE image of MB2 shows the absence of WSP which is attributed to higher solidification rate.

(Tb,Dy)Fe<sub>2</sub> from liquid is lower than 18 cm/h, the lowest zoning rate employed in this study. In MB1 experiment, however, the temperature gradient prevalent was lower as compared to the zoning experiment and hence, the  $V_{tr}$  may be higher than rate of solidification (14 cm/h), favoring the formation of (Tb,Dy)Fe<sub>3</sub> right from the initial stage of solidification. In contrast, during the initial period of solidification of the MB2 sample, the rate of solidification employed (70 cm/h) exceeds  $V_{tr}$  resulting in the formation of (Tb,Dy)Fe<sub>2</sub> congruently from the liquid. Thus, the  $V_{tr}$  value lies between 14 and 70 cm/h for the thermal gradient that prevailed during the MB experiments. However, the temperature gradient starts decreasing at regions away from the chilled zone, and at some distance away from the chilled surface, the solidification rate becomes lower than  $V_{tr}$  and as a consequence (Tb,Dy)Fe<sub>3</sub> phase starts forming as primary phase (MB2 sample).

### 1. Widmanstätten precipitate

A network of fine platelet-type Widmanstätten precipitate (WSP), which is distributed in the matrix of (Tb,Dy)Fe<sub>2</sub> phase is noticed in the CC sample (Fig. 5). A similar network of fine precipitate has been noticed in all sections of MB1 also. Interestingly, these precipitates were not observed in MB2 and in all the zoned (Z1, Z2, and Z3) samples. Earlier investigators<sup>14,16,17</sup> have identified these precipitates to be (Tb,Dy)Fe<sub>3</sub> phase, describing its formation on the basis of existence of a narrow solubility range for the Laves phase towards the rare earth rich side. As the solidification progresses the precipitates of (Tb,Dy)Fe<sub>3</sub> are formed preferably on the facets of {111} of (Tb,Dy)Fe<sub>2</sub> phase leading to the formation of WSP. This being a diffusion assisted process the reaction kinetics has a strong dependency on the rate of

TABLE I. Inferred solidification sequence of the Tb<sub>0.3</sub>Dy<sub>0.7</sub>Fe<sub>1.95</sub> alloy under different growth conditions.

Under equilibrium condition according to phase diagram	CC and MB1 samples	MB2, Z1, Z2, and Z3 samples
L	L	L
↓	↓	↓
L+(Tb,Dy)Fe <sub>3</sub>	L+(Tb,Dy)Fe <sub>3</sub>	L + (Tb,Dy)Fe <sub>2</sub>
↓	↓	↓
L + (Tb,Dy)Fe <sub>2</sub>	L + (Tb,Dy)Fe <sub>3</sub> + (Tb,Dy)Fe <sub>2</sub>	(Tb,Dy)-rich + (Tb,Dy)Fe <sub>2</sub>
↓	↓	↓
(Tb,Dy)-rich + (Tb,Dy)Fe <sub>2</sub>	(Tb,Dy)-rich (Tb,Dy)Fe <sub>3</sub> + (Tb,Dy)Fe <sub>2</sub>	(Tb,Dy)Fe <sub>2</sub>
	+	
	(Tb,Dy)Fe <sub>2</sub>	WSP (Tb,Dy)Fe <sub>3</sub>

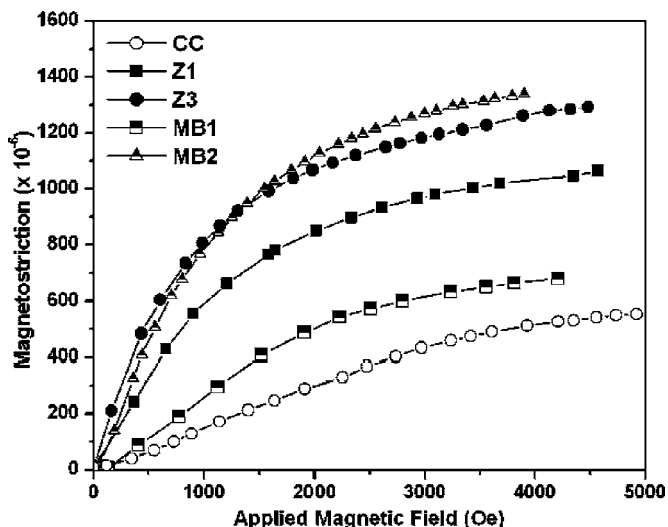


FIG. 6. The variation of magnetostriction as a function of applied dc magnetic field for the conventionally cast and directionally solidified samples.

cooling. It is evident from this study that the formation of WSP is difficult either at a higher rate of solidification or at higher temperature gradient (or both). Therefore, slow rate of solidification would aid diffusion and cause precipitation of  $(\text{Tb}, \text{Dy})\text{Fe}_3$  as observed in the CC and MB1 samples. On the contrary, the diffusion kinetics is inhibited due to higher temperature gradient in the zoned samples (Z1, Z2, Z3) and due to higher solidification rate in MB2 sample. Hence, formation of WSP was found suppressed in all the zoned (Z1, Z2, Z3) and MB2 samples.

## B. Magnetostriction

The plots of magnetostriction ( $\lambda$ ) versus applied dc magnetic field ( $H$ ) for CC and directionally solidified (Z1, Z3, MB1, and MB2) samples are given in Fig. 6. The improvement brought about in magnetostriction by directional solidification is remarkably high compared to that obtained in the conventionally cast condition. This is attributed to (i) the preferred grain orientation as a result of directional solidification and in accordance with the earlier reported values by several investigators<sup>9-11,18-20</sup> and (ii) suppression of  $(\text{Tb}, \text{Dy})\text{Fe}_3$  phase.

When comparing the effect of different solidification rates adopted in the study, it is inferred that a higher rate of solidification within those employed in the present study is beneficial to realize large magnetostriction and also a sharp rise in the magnetostriction from zero. This is one of the important quality factors of the material for the transducer applications. Considering that the solidification rates are comparable for Z1 and MB1 on one hand, and Z3 and MB2 on the other, the magnetostriction values are also expected to be closer for these two sets of samples. However, an examination of the magnetostriction plots (Fig. 6) of these samples reveals that the high “initial magnetostriction” (for  $H \sim$  up to 1.0 kOe) is achievable at lower solidification rates in zoning than in the modified Bridgman technique. Another interesting observation is that the difference in the value of magnetostriction among the zoned samples grown at different so-

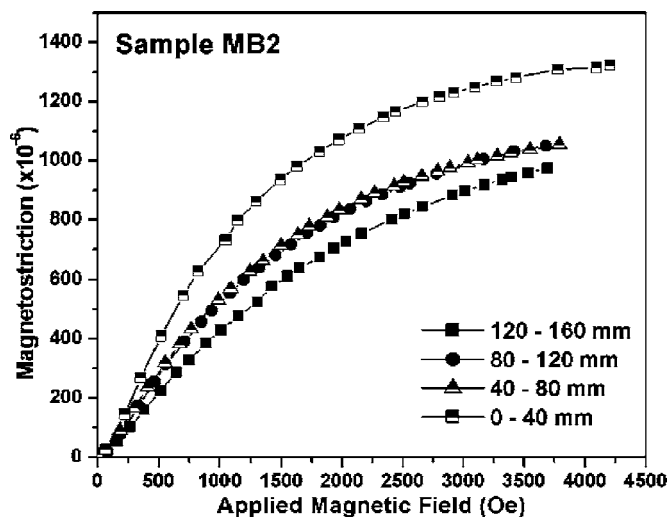


FIG. 7. Plot of magnetostriction as a function of applied dc magnetic field for the longitudinal sections of the MB2 rod from the chilled end.

lidification rates is small whereas it is remarkably high for the samples (MB1 and MB2) grown by Bridgman technique. The magnetostriction values obtained for Z3 and MB2 samples are comparable to that reported earlier by the other researchers.<sup>11,12,18</sup>

The consistency of magnetostriction in the entire length of the sample was evaluated for Z3 and MB2 samples by plotting  $\lambda$  versus applied field for different sample sections cut along the cylindrical axis of the solidified rod. While very little deviation ( $<1\%$ ) in magnetostriction was noticed in the zoned samples, considerable variation was observed (Fig. 7) for the MB2 sample, being maximum at the initially solidified section (chill end) and decreasing as a function of distance from the chilled end. A similar trend has been noticed in the value of initial magnetostriction too. While relating the observed variation of magnetostriction to the microstructure of the corresponding sections of the samples, the appearance of  $(\text{Tb}, \text{Dy})\text{Fe}_3$  phase at 40 mm away from the chilled surface seems to be the main cause for the decrease in the magnetostriction.

The systematic improvement in the magnetostriction as a function of solidification rate implies that if  $(\text{Tb}, \text{Dy})\text{Fe}_2$  congruently solidifies from the liquid, the magnetostriction measured in such samples is high. On the contrary, solidification through the peritectic reaction with the formation of primary crystallites of  $(\text{Tb}, \text{Dy})\text{Fe}_3$  as is the case in the CC, MB1 and also in MB2 at some distance away from the chilled zone, leads to relatively low magnetostriction values. According to Verhoeven *et al.*,<sup>21</sup> the magnetostriction depends on the  $(\text{Tb}, \text{Dy})/\text{Fe}$  ratio of the Laves phase. From the investigation presented here it is surmised that this ratio approaches the stoichiometric  $(\text{Tb}, \text{Dy})\text{Fe}_2$  if the Laves phase is formed by direct crystallization from the liquid through congruent solidification. However, if the solidification leads to the formation of  $(\text{Tb}, \text{Dy})\text{Fe}_3$ , then the ratio  $(\text{Tb}, \text{Dy})/\text{Fe}$  deviates from the stoichiometry and the magnetostriction consequently decreases. So the  $(\text{Tb}, \text{Dy})/\text{Fe}$  ratio has an effect on magnetoelastic coupling responsible for the rhombohedral distortion of the cubic Laves phase. It has been reported<sup>22,23</sup> that the

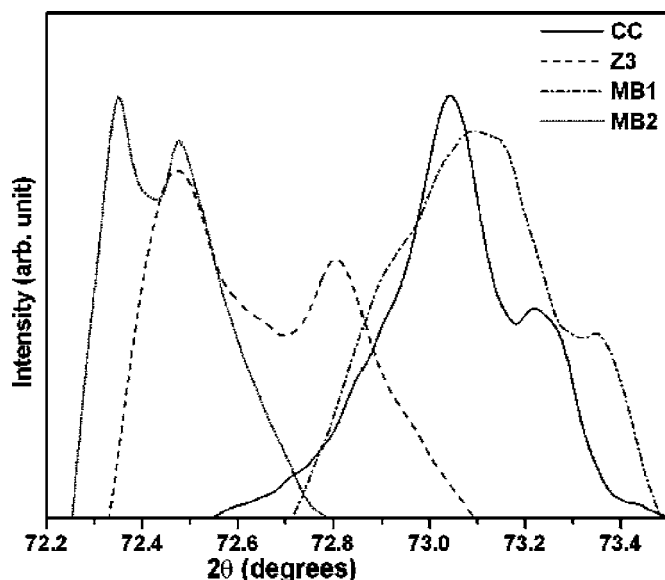


FIG. 8. Profile of (440) XRD peaks of the  $(\text{Tb,Dy})\text{Fe}_2$  phase observed in conventionally cast and directionally solidified samples of  $\text{Tb}_{0.3}\text{Dy}_{0.7}\text{Fe}_{1.95}$ .

splitting of the (440) peak in the XRD pattern can be taken as a measure for the rhombohedral distortion of the unit cell of  $(\text{Tb,Dy})\text{Fe}_2$  phase. The XRD peaks of (440) corresponding to the conventionally cast and directionally solidified samples (Z3, MB1, and MB2) are shown in Fig. 8. The split is markedly prominent for the samples (Z3 and MB2) directionally solidified at higher growth rates, whereas it is less prominent in the sample CC and in the sample (MB1) grown at low solidification rate. This corroborative evidence also supports the understanding derived from the microstructural evaluation of conventionally cast and directionally solidified samples that large magnetostriction can be obtained if the  $(\text{Tb,Dy})\text{Fe}_2$  phase is formed by congruent solidification:

#### IV. CONCLUSIONS

The compound  $\text{Tb}_{0.3}\text{Dy}_{0.7}\text{Fe}_{1.95}$  was conventionally cast and also directionally solidified using zoning and modified Bridgman techniques. The microstructure of the directionally solidified samples was studied using optical microscope, SEM/EDS, and correlated with the magnetostriction measured by resistance strain gauges. The results are summarized as follows:

- (1) At higher temperature gradient and solidification rate, formation of properitectic  $(\text{Tb,Dy})\text{Fe}_3$  phase is not kinetically favored and  $(\text{Tb,Dy})\text{Fe}_2$  phase forms congruently from the liquid.
- (2) Formation of fine WSP-type  $(\text{Tb,Dy})\text{Fe}_3$  phase occurs only if the solidification rate and temperature gradient are sufficiently low to allow diffusion and reach equilibrium condition.

- (3) Deviation in the  $(\text{Tb,Dy})/\text{Fe}$  ratio of the Laves phase is attributed to be the reason for the variation in the magnetostriction measured (at a given bias field) on the samples solidified under different solidification conditions. Larger deviation in  $(\text{Tb,Dy})/\text{Fe}$  ratio occurs if  $(\text{Tb,Dy})\text{Fe}_2$  phase forms through the peritectic reaction  $L + (\text{Tb,Dy})\text{Fe}_2 \rightarrow (\text{Tb,Dy})\text{Fe}_3$ , resulting in lower magnetostriction ( $\lambda$ ).
- (4) The formation of  $(\text{Tb,Dy})\text{Fe}_2$  by congruent solidification due to higher solidification rate and higher thermal gradient, either one or both, essentially results in realizing larger magnetostriction, and is attributed to the  $(\text{Tb,Dy})/\text{Fe}$  ratio of Laves phase being closer to that of stoichiometric  $(\text{Tb,Dy})\text{Fe}_2$ .

#### ACKNOWLEDGMENTS

The authors thank Defence R&D Organization for the financial support and the Director, DMRL for his encouragement and for permission to publish this work.

- <sup>1</sup>A. E. Clark, AIP Conf. Proc. **10**, 149 (1973).
- <sup>2</sup>D. C. Jiles, J. Phys. D **27**, 1 (1994).
- <sup>3</sup>O. D. McMasters, J. D. Verhoeven, and E. D. Gibson, J. Magn. Magn. Mater. **54–57**, 849 (1986).
- <sup>4</sup>J. D. Verhoeven, E. D. Gibson, O. D. McMasters, and H. H. Baker, Metall. Trans. A **18A**, 223 (1987).
- <sup>5</sup>T. Funayama, T. Kobayashi, I. Sakai, and M. Sahashi, Appl. Phys. Lett. **61**, 114 (1992).
- <sup>6</sup>L. Wu, W. Zhan, X. Own, and X. Chen, J. Magn. Magn. Mater. **139**, 335 (1995).
- <sup>7</sup>T. Ma, C. Jiang, X. Xu, H. Zhang, and H. Xu, J. Magn. Magn. Mater. **292**, 317 (2005).
- <sup>8</sup>G. Wu, X. Zhao, J. Wang, J. Li, K. Jia, and W. Zhan, Appl. Phys. Lett. **67**, 2005 (1995).
- <sup>9</sup>W. Mei, T. Okane, T. Umeda, and S. Zhou, J. Alloys Compd. **248**, 151 (1997).
- <sup>10</sup>C. Ji, J. Li, W. Ma, and Y. Zhou, J. Alloys Compd. **333**, 291 (2002).
- <sup>11</sup>Y. Zhao, C. Jiang, H. Zhang, and H. Xu, J. Alloys Compd. **354**, 263 (2003).
- <sup>12</sup>K. R. Dhilsha, G. Markandeyulu, and K. V. S. Rama Rao, J. Appl. Phys. **87**, 7208 (1991).
- <sup>13</sup>A. S. Vandergoot and K. H. J. Buschow, J. Less-Common Met. **21**, 151 (1970).
- <sup>14</sup>M. P. Dariel, J. T. Holthus, and M. R. Pickus, J. Less-Common Met. **45**, 91 (1976).
- <sup>15</sup>T. Umeda, T. Okane, and W. Kurz, Acta Mater. **44**, 4209 (1996).
- <sup>16</sup>P. Westwood, J. S. Abell, H. Clarke, and K. C. Pitman, J. Appl. Phys. **64**, 5414 (1988).
- <sup>17</sup>P. Westwood, J. S. Abell, and K. C. Pitman, J. Appl. Phys. **67**, 4998 (1990).
- <sup>18</sup>J. D. Snodgrass and O. D. McMaster, J. Alloys Compd. **258**, 24 (1997).
- <sup>19</sup>T. Ma, C. Jiang, X. Xu, and H. Xu, J. Alloys Compd. **388**, 34 (2005).
- <sup>20</sup>J. C. Yan, X. Q. Xie, S. Q. Yang, and S. Y. He, J. Magn. Magn. Mater. **223**, 27 (2001).
- <sup>21</sup>J. D. Verhoeven, O. D. McMasters, J. D. Ostenson, and E. D. Gibson, J. Appl. Phys. **66**, 772 (1989).
- <sup>22</sup>W. J. Ren, S. W. Or, H. L. W. Chan, W. F. Li, X. G. Zhao, X. P. Song, and Z. D. Zhang, IEEE Trans. Magn. **40**, 2766 (2004).
- <sup>23</sup>W. J. Ren, S. W. Or, H. L. W. Chan, W. F. Li, X. G. Zhao, J. J. Liu, and Z. D. Zhang, IEEE Trans. Magn. **40**, 2772 (2004).